Modeling and Analysis of Sector Clock Bias Mismatch for Navigation with Cellular Signals

Joe Khalife[1] and Zaher M. Kassas[2]

***Abstract*— The clock bias in different sectors of a cellular base transceiver station (BTS) cell is studied. A dynamical model relating the clock biases in different BTS sectors is identified and validated experimentally. A theoretical estimation error lower bound due to the discrepancy between sector clock biases is derived and demonstrated against Monte Carlo simulation runs. Experimental results of an unmanned aerial vehicle (UAV) navigating exclusively with cellular code division multiple access signals are presented. These results demonstrate a 10.51m reduction in the UAV's position estimation error due to incorporating the developed sector mismatch model into the estimation framework.**

I. Introduction

Over the past decade, research in navigation via signals of opportunity (SOPs) has revealed their potential as an alternative or a complement to global navigation satellite system (GNSS). Such signals include AM/FM radio [1], iridium satellites [2], cellular [3], [4], digital television [5], and Wi-Fi [6]. The literature on SOPs answers theoretical questions on the observability and estimability of the SOP signal landscape [7], motion planning in the SOP signal landscape for optimal information gathering [8]–[10], and collaborative SOP landscape map building [11]. Moreover, a number of experimental demonstrations have shown receiver localization and timing via SOPs [12]–[16].

There are several challenges associated with using SOPs for navigation, most notably the unavailability of: (1) specialized receivers capable of extracting states and parameters of interest from received signals for navigation purposes and (2) sources of error analysis for navigating via different classes of SOPs. A critical source of error in SOP-based navigation is the mismatch in the dynamics and/or observation models. An agent entering a new signal landscape cannot assume the availability of high fidelity models describing the SOP landscape dynamics. As such, adaptive estimation algorithms and estimation error bounds due to model mismatch must be developed. In [17], adaptive filters for estimating the SOP's process noise covariance pertaining to the clock error states (bias and drift) of cellular SOPs were presented. In [3], a new error source corresponding to cellular code division multiple access (CDMA) signals was revealed, namely bias mismatch for different sectors within the same cellular base transceiver station (BTS) cell. It is important to note that while these errors are not harmful for communication purposes, they severely degrade the navigation performance if they are not modeled and accounted for appropriately.

Ideally, the clocks of all sectors within a particular BTS cell should be driven by the same oscillator, which implies that the same clock bias should be observed in all sectors of the same cell. However, factors such as unknown distance between the phase-center of the sector antennas and delays due to radio frequency (RF) connectors and other components (e.g., cabling, filters, amplifiers, etc.) cause the clock biases corresponding to different BTS sectors to be slightly different. This behavior was consistently observed in experimentally collected data [18].

This discrepancy can be particularly harmful for navigation purposes in two scenarios. In the first scenario, an agent that has no knowledge of its own states, nor has access to GNSS, is present in a cellular CDMA environment and is making pseudorange measurements to BTSs nearby. The agent has access to estimates of the BTSs' states through a central database. These estimates could be produced through stationary mapping agents or crowdsourced from mobile agents in the environment. In some cases, while estimates of the BTS sector in which the navigating agent is located may not be available, estimates of a *different* sector of the same BTS cell may be available in the database. If the navigating agent uses such estimates, the discrepancy between the sector clock biases will introduce errors on the order of tens of meters in the agent's position estimate and tens of nanoseconds in the agent's clock bias estimate. A second scenario where this discrepancy must be accounted for is when the agent is navigating in a simultaneous localization and mapping framework and is transitioning from one sector of the BTS to another.

This paper makes two contributions: (1) it identifies a stochastic dynamic model for the clock bias mismatch in different sectors of a BTS cell and (2) it derives estimation error bounds due to the discrepancy between the sectors' clock biases. Simulation and experimental results are presented demonstrating the paper's contributions.

The remainder of the paper is organized as follows. Section II discusses a mapper/navigator framework for navigation with cellular signals. Section III develops and validates a stochastic dynamic model capturing the error between the clock biases of different sectors of the same BTS. Section IV characterizes the estimation performance under such errors. Section V presents experimental results demonstrating estimation error reduction due to incorporating the developed models. Concluding remark are provided in Section VI.

This work was supported in part by the Office of Naval Research (ONR) under Grant N00014-16-1-2305.

[1] Graduate student, Department of Electrical & Computer Engineering, University of California, Riverside, USA, jkhalife@ece.ucr.edu.

[2] Assistant professor, Department of Electrical & Computer Engineering, University of California, Riverside, USA, zkassas@ieee.org.

II. Mapper/Navigator Framework for Cellular-Based Navigation

This section describes a framework for navigating with cellular signals. It consists of two agents: a mapping node, referred to as the mapper, and a navigating node, referred to as the navigator. The mapper is assumed to have full knowledge of its position and clock states (by having access to GNSS signals, for example). Both nodes are equipped with a cellular receiver that is capable of producing pseudorange measurements to nearby BTSs [3].

A. Pseudorange Measurement Model

By making pseudorange observations to $N \geq 3$ BTSs, one may estimate the two-dimensional (2-D) position and clock bias of the navigator, provided that the BTS locations and their clock biases are known. The state of the navigator is defined as $\boldsymbol{x}_n \triangleq \left[\boldsymbol{r}_n^{\mathsf{T}}, c\delta t_n\right]^{\mathsf{T}}$, where $\boldsymbol{r}_n = [x_n, y_n]^{\mathsf{T}}$ is the position vector of the navigator, δt_n is the navigator's clock bias, and c is the speed-of-light. Similarly, the state of the ith BTS is defined as $\boldsymbol{x}_{s_i} \triangleq \left[\boldsymbol{r}_{s_i}^{\mathsf{T}}, c\delta t_{s_i}\right]^{\mathsf{T}}$, where $\boldsymbol{r}_{s_i} = [x_{s_i}, y_{s_i}]^{\mathsf{T}}$ is the position vector of the ith BTS and δt_{s_i} is the clock bias. The pseudorange measurement to the ith BTS at time k, $\rho_i(k)$, is given by

$$\rho_i(k) = h_i\left[\boldsymbol{x}_n(k), \boldsymbol{x}_{s_i}(k)\right] + v_i(k), \tag{1}$$

where $h_i\left[\boldsymbol{x}_n(k), \boldsymbol{x}_{s_i}(k)\right] \triangleq \|\boldsymbol{r}_n(k) - \boldsymbol{r}_{s_i}\| + c \cdot [\delta t_n(k) - \delta t_{s_i}(k)]$ and v_i is the observation noise, which is modeled as a zero-mean white Gaussian random sequence with variance σ_i^2 [7]. The navigator's state can be readily estimated by solving a weighted nonlinear least-squares (WNLS) problem.

B. BTS State Estimation and Modified Pseudorange Model

Consider a mapper with knowledge of its own state vector to be present in the navigator's environment. The mapper's objective is to estimate the BTSs' position and clock bias states and share these estimates with the navigator through a central database. It is assumed that the mapper has been estimating the SOP BTSs' states for a sufficiently long period of time and that the position state estimate uncertainties had become negligible. The position state estimates are physically verifiable (through surveying or satellite images, for example), at which point these estimates are assumed to match the true states and are subsequently stored in the database. Unlike the position state estimates, the clock bias state estimates are more difficult to verify and are time-varying. Therefore, in the sequel, it is assumed that the mapper is only estimating the BTSs' clock bias states, and is sharing these estimates $\left\{\hat{\delta t}_{s_i}\right\}_{i=1}^{N}$ and their associated error variances $\left\{\sigma^2_{\delta t_{s_i}}\right\}_{i=1}^{N}$ with the navigator (see Fig. 1).

Since the navigator is using the estimate of the BTS clock bias produced by the mapper, the pseudorange measurement made by the navigator on the ith BTS is modified to

$$\rho_i(k) = \hat{h}_i(k) + \eta_i(k), \tag{2}$$

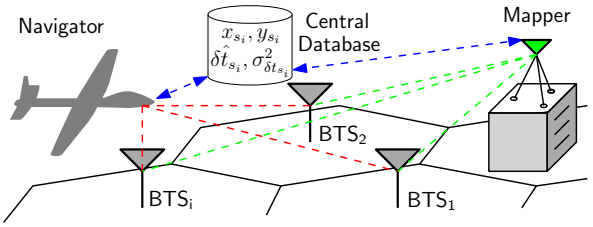

Fig. 1. Mapper and navigator in a cellular environment.

where $\hat{h}_i(k) \triangleq h_i\left[\boldsymbol{x}_n(k), \hat{\boldsymbol{x}}_{s_i}(k)\right]$, $\hat{\boldsymbol{x}}_{s_i}(k) = \left[\boldsymbol{r}_{s_i}^{\mathsf{T}}, c\hat{\delta t}_{s_i}(k)\right]^{\mathsf{T}}$ and η_i is a zero-mean white Gaussian random sequence with variance $\sigma^2_{\eta_i} = \sigma_i^2 + c^2\sigma^2_{\delta t_{s_i}}$ that models the overall uncertainty in the measurement.

III. Modeling of the Clock Bias Discrepancy between Different Sectors of a BTS Cell

The sources of error considered so far pertain to measurement noise and to the estimation error inherent to the BTSs' clock bias estimates produced by the mapper. However, an additional source of error due to the discrepancy between the clock biases corresponding to different BTS sectors within the same cell was observed [3]. In this section, a stochastic dynamic model for this discrepancy is identified.

A. Detecting the Discrepancy Between Sectors' Clock Biases

In order to detect the discrepancy between sectors' clock biases, a cellular CDMA receiver was placed at the border of two sectors of a BTS cell and was drawing pseudorange measurements from both sector antennas. The receiver had full knowledge of its state and of the BTS' position. Subsequently, the receiver solved for the BTS clock biases $\delta t_{s_i}^{(p_i)}$ and $\delta t_{s_i}^{(q_i)}$ observed in sectors p_i and q_i, respectively. A realization of $\delta t_{s_i}^{(p_i)}$ and $\delta t_{s_i}^{(q_i)}$ is depicted in Fig. 2.

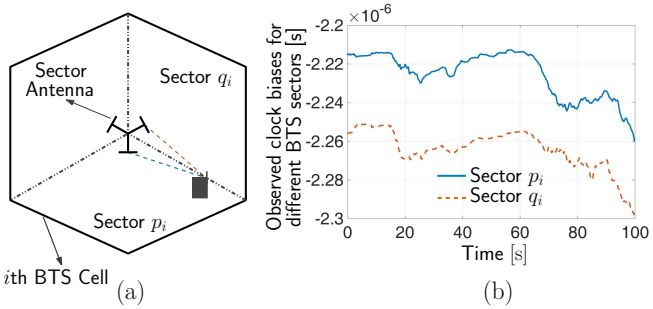

Fig. 2. (a) A cellular CDMA receiver placed at the border of two sectors of a BTS cell, making pseudorange observations on both sector antennas simultaneously. The receiver has knowledge of its own states and has knowledge of the BTS position states. (b) Observed BTS clock bias corresponding to two different sectors.

Fig. 2 suggests that the clock biases $\delta t_{s_i}^{(p_i)}$ and $\delta t_{s_i}^{(q_i)}$ can be related through

$$\delta t_{s_i}^{(q_i)}(k) = \delta t_{s_i}^{(p_i)}(k) + \left[1 - 1_{q_i}(p_i)\right]\epsilon_i(k),$$

where ϵ_i is a random sequence that models the discrepancy between the sectors' clock biases and

$$1_{q_i}(p_i) = \begin{cases} 1, & \text{if } p_i = q_i, \\ 0, & \text{otherwise,} \end{cases}$$

is the indicator function. In what follows, a stochastic dynamic model for ϵ_i is identified.

B. Model Identification

It is hypothesized that the discrepancy $\epsilon_i(k) = \delta t_{s_i}^{(q_i)}(k) - \delta t_{s_i}^{(p_i)}(k)$ for $p_i \neq q_i$ adheres to an autoregressive (AR) model of order n, which can be expressed as [19]

$$\epsilon_i(k) + \sum_{j=1}^{n} \alpha_j \epsilon_i(k-j) = \zeta(k),$$

where ζ is a white sequence. The objective is to find the order n and the coefficients $\{\alpha_j\}_{j=1}^n$ that will minimize the sum of the squared residuals $\sum_{l=0}^{k} \zeta^2(l)$. To find the order n, several AR models were identified and for a fixed order, a least-squares estimator was used to solve for $\{\alpha_j\}_{j=1}^n$. It was noted that the sum of the squared residuals corresponding to each $n \in \{1, \ldots, 10\}$ were comparable, suggesting that the minimal realization of the AR model is of first-order. For $n = 1$, it is found that $\alpha_1 = -(1-\beta)$, where $0 < \beta << 1$ (on the order of 8×10^{-5} to 3×10^{-4}). This implies that ϵ_i is an exponentially correlated random variable (ECRV), with $\exp\left(-\frac{T}{\tau}\right) = 1 - \beta$, where T is the sampling time and τ is the time constant of the continuous-time model of the discrepancy. Experimental data collected over five-minute time spans shows that $\frac{1}{\tau} \to 0$ for different carriers, at different times, and in different locations. In particular, $\frac{1}{\tau} = \{2.08, 1.66, 1.77, 1.70, 1.39, 2.53\} \times 10^{-4}$ for the six data sets reported in [18]. Consequently, $\alpha_1 \approx -1$, implying that ϵ_i evolves according to a random walk given by

$$\epsilon_i(k+1) = \epsilon_i(k) + \zeta(k). \tag{3}$$

Fig. 3 shows a realization of ϵ_i and the corresponding residual ζ.

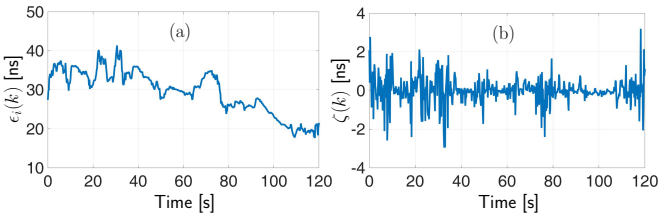

Fig. 3. (a) A realization of the discrepancy ϵ_i between the observed clock biases of two BTS sectors and (b) the corresponding residual ζ.

C. Model Validation

The identified model in (3) was validated through residual analysis [19]. To this end, the autocorrelation function (acf) and power spectral density (psd) of the residual error e_i defined as the difference between the measured data ϵ_i' and predicted value from the identified model ϵ_i in (3), i.e., $e_i \triangleq \epsilon_i' - \epsilon_i$, were computed. Fig. 4 shows the acf and psd of e_i computed from a different realization of ϵ_i. The psd was computed using Welch's method [20]. It can be seen from Fig. 4 that the residual error e_i is nearly white; hence, the identified model is capable of describing the true system.

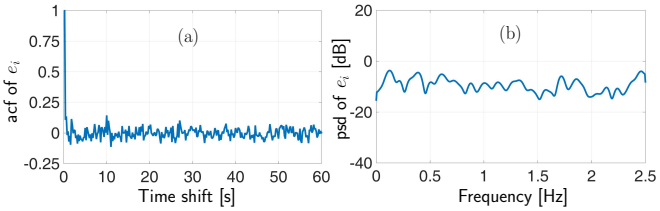

Fig. 4. The (a) acf and (b) psd of e_i with a sampling frequency of 5 Hz.

D. Residual Statistics Characterization

Next, the probability density function (pdf) of ζ will be characterized, assuming that ζ is an ergodic process. It was found that the Laplace distribution best matches the actual distribution of ζ obtained from experimental data, i.e., the pdf of ζ is given by $p(\zeta) = \frac{1}{2\lambda} \exp\left(-\frac{|\zeta - \mu|}{\lambda}\right)$, where μ is the mean of ζ and λ is the parameter of the Laplace distribution, which can be related to the variance by $\sigma_\zeta^2 = 2\lambda^2$. A maximum likelihood estimator (MLE) was adopted to calculate the parameters μ and λ of $p(\zeta)$ [21]. Fig. 5 shows the actual distribution of the data along with the estimated pdf.

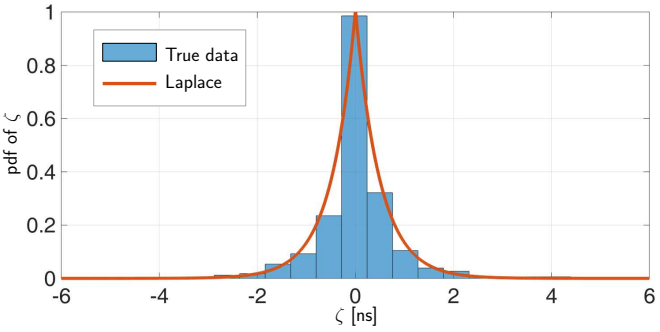

Fig. 5. Distribution of ζ from experimental data and the estimated Laplace pdf via MLE.

It was noted that $|\mu| \approx 0$ from several batches of collected experimental data; therefore, ζ is appropriately modeled as a zero-mean white Laplace-distributed random sequence with variance $2\lambda^2$. From (3), $\epsilon_i(k)$ can be expressed as $\epsilon_i(k) = \epsilon_i(0) + \sum_{l=0}^{k-1} \zeta(l)$, where $\epsilon_i(0)$ is the known initial discrepancy. Without loss of generality, $\epsilon_i(0)$ is assumed to be zero. The central limit theorem asserts that the pdf of ϵ_i converges to a Gaussian pdf. It was noted that the convergence happens for $k \geq 9$. Therefore, for $k \geq 9$, ϵ_i is modeled as Gaussian with mean $k\mu \approx 0$ and variance $2k\lambda^2$.

IV. Performance Characterization in the Presence of Sector Clock Bias Discrepancies

In this section, the pseudorange model (2) is refined to account for the discrepancy between sector clock biases. Also, an analytical lower bound on the determinant of the estimation error covariance in the presence of clock bias discrepancy is derived.

A. Pseudorange Model in the Presence of Sector Clock Bias Discrepancies

The pseudorange measured by the navigator in sector q_i of the ith BTS when the mapper is in sector p_i is given by

$$\rho_i^{(q_i)}(k) = \hat{h}_i^{(p_i)}(k) + \eta_i(k) - [1 - 1_{q_i}(p_i)] \cdot [c\epsilon_i(k)], \quad (4)$$

where $\hat{h}_i^{(p_i)}(k) \triangleq h_i\left[\boldsymbol{x}_r(k), \hat{\boldsymbol{x}}_{s_i}^{(p_i)}(k)\right]$ and $\hat{\boldsymbol{x}}_{s_i}^{(p_i)}(k) = \left[\boldsymbol{r}_{s_i}^{\mathsf{T}}, c\hat{\delta t}_{s_i}^{(p_i)}(k)\right]^{\mathsf{T}}$. It is assumed that $\sigma_{\eta_i}^2 = \sigma_\eta^2$ for $i = 1, \ldots, N$. In the remainder of this section, the mapper and navigator are assumed to be drawing pseudorange measurements from N BTSs, N_s of which have a mismatch between the mapper and navigator sectors. Without loss of generality, the set of pseudoranges are ordered such that the first N_s measurements correspond to the ones coming from the BTSs with sector mismatch between the mapper and navigator. Hence, (4) can be expressed as

$$\boldsymbol{\rho}(k) = \hat{\boldsymbol{h}}(k) + \boldsymbol{w}(k), \quad (5)$$

where $\hat{\boldsymbol{h}}(k) \triangleq \left[\hat{h}_1^{(p_1)}(k), \ldots, \hat{h}_N^{(p_N)}(k)\right]^{\mathsf{T}}$, $\boldsymbol{w}(k) \triangleq c\boldsymbol{\epsilon}(k) + \boldsymbol{\eta}(k)$, $\boldsymbol{\epsilon}(k) \triangleq [\epsilon_1(k), \ldots, \epsilon_{N_s}(k), 0, \ldots, 0]^{\mathsf{T}}$, and $\boldsymbol{\eta} \triangleq [\eta_1(k), \ldots, \eta_N(k)]^{\mathsf{T}}$. The term $\boldsymbol{w}(k)$ captures the errors due to measurement noise, mapper estimation errors, and discrepancies between the sectors' clock biases. It is modeled as a zero-mean Gaussian random vector with a covariance matrix $\mathbf{R}_k$ given by

$$\mathbf{R}_k = \begin{bmatrix} \left(\sigma_\eta^2 + 2kc^2\lambda^2\right)\mathbf{I}_{N_s \times N_s} & \mathbf{0}_{N_s \times (N-N_s)} \\ \mathbf{0}_{(N-Ns)\times N_s} & \sigma_\eta^2 \mathbf{I}_{(N-N_s)\times(N-N_s)} \end{bmatrix}. \quad (6)$$

B. Navigation Solution and Jacobian Re-parametrization

Given the measurement model in (5), one can solve for the state of the navigator state using an iterative WNLS. Since only a point solution is considered, the time argument k will be dropped for simplicity of notation. At steady-state, an estimate for the navigator state $\hat{\boldsymbol{x}}_n$ is obtained along with an estimation error covariance $\mathbf{P} = \left(\mathbf{H}^{\mathsf{T}}\mathbf{R}^{-1}\mathbf{H}\right)^{-1}$, where $\mathbf{H}$ is the Jacobian matrix evaluated at $\hat{\boldsymbol{x}}_n$. The matrix $\mathbf{H}$ can be expressed as $[\mathbf{G} \quad \mathbf{1}_N]$, where $\mathbf{G} \triangleq [\boldsymbol{x} \quad \boldsymbol{y}]$, $\boldsymbol{x} \triangleq [x_1, \ldots, x_N]^{\mathsf{T}}$, $x_i = \frac{x_n - x_{s_i}}{\|\boldsymbol{r_n} - \boldsymbol{r_{s_i}}\|}$, $\boldsymbol{y} \triangleq [y_1, \ldots, y_N]^{\mathsf{T}}$, $y_i = \frac{y_n - y_{s_i}}{\|\boldsymbol{r_n} - \boldsymbol{r_{s_i}}\|}$, and $\mathbf{1}_N \triangleq [1, \ldots, 1]^{\mathsf{T}}$. The vectors $\boldsymbol{x}$ and $\boldsymbol{y}$ can be re-parameterized by the bearing angle θ_i between the navigator and the ith BTS, as shown in Fig. 6(a). Hence, $\boldsymbol{x} = [\cos\theta_1, \ldots, \cos\theta_N]^{\mathsf{T}}$ and $\boldsymbol{y} = [\sin\theta_1, \ldots, \sin\theta_N]^{\mathsf{T}}$.

C. Optimal Performance in the Presence of Sector Mismatch

In this subsection, a lower bound on the determinant of the estimation error covariance is derived for the case of pseudorange measurements with a measurement covariance matrix given in (6). For identically distributed measurement noise, i.e., $\mathbf{R} = \sigma^2\mathbf{I}_{N\times N}$, where $\mathbf{R}$ is the measurement noise covariance and σ^2 is the measurement noise variance, the BTS configuration that achieves the minimum determinant of the estimation covariance is when the line-of-sight (LOS) vectors from the receiver to the $N \geq 3$ BTSs form a regular polyhedron around the receiver [22]. The angles $\{\theta_i\}_{i=1}^N$ corresponding to this configuration are given by $\{\theta_i = \frac{2\pi}{N}i + \theta_0\}_{i=1}^N$, where θ_0 is an arbitrary offset angle. In the presence of sector mismatch, the measurement noise is not identically distributed anymore. In this case, the optimal configuration is relaxed so that the LOS vectors from the receiver to the set of $N_s \geq 3$ BTSs with sector mismatch form a regular polygon and the LOS vectors to the remaining $N - Ns \geq 3$ BTSs with no sector mismatch also form another regular polygon. This configuration can be described by

$$\theta_i = \begin{cases} \frac{2\pi}{N_s}i + \theta_0', & i = 1, \ldots, N_s, \\ \frac{2\pi}{N-N_s}(i - N_s) + \theta_0, & i = N_s + 1, \ldots, N, \end{cases} \quad (7)$$

where θ_0' is an arbitrary offset angle, as shown in Fig. 6(b).

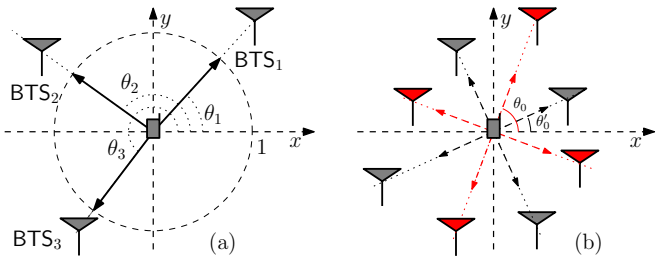

Fig. 6. (a) Re-parametrization of the unit line-of-sight (LOS) vectors by the bearing angles. (b) Optimal distribution of the BTSs around the receiver (red: BTSs with sector mismatch, gray: BTSs with no sector mismatch).

For a measurement covariance $\mathbf{R}_k$ given in (6), the information matrix $\mathbf{M} = \mathbf{P}^{-1} = \mathbf{H}^{\mathsf{T}}\mathbf{R}^{-1}\mathbf{H}$ is given by

$$\mathbf{M} = \begin{bmatrix} \boldsymbol{x}^{\mathsf{T}}\mathbf{R}_k^{-1}\boldsymbol{x} & \boldsymbol{x}^{\mathsf{T}}\mathbf{R}_k^{-1}\boldsymbol{y} & \boldsymbol{x}^{\mathsf{T}}\mathbf{R}_k^{-1}\mathbf{1}_N \\ \bar{\boldsymbol{y}}^{\mathsf{T}}\mathbf{R}_k^{-1}\bar{\boldsymbol{x}} & \boldsymbol{y}^{\mathsf{T}}\mathbf{R}_k^{-1}\boldsymbol{y} & \boldsymbol{y}^{\mathsf{T}}\mathbf{R}_k^{-1}\mathbf{1}_N \\ \mathbf{1}_N^{\mathsf{T}}\mathbf{R}_k^{-1}\boldsymbol{x} & \mathbf{1}_N^{\mathsf{T}}\mathbf{R}_k^{-1}\boldsymbol{y} & \mathbf{1}_N^{\mathsf{T}}\mathbf{R}_k^{-1}\mathbf{1}_N \end{bmatrix}.$$

Given the configuration in (7) and the following properties for this configuration [22]

$$\textstyle\sum_{l=1}^L \cos^2\theta_l = \sum_{l=1}^L \sin^2\theta_l = \frac{L}{2}, \quad (8)$$

$$\textstyle\sum_{l=1}^L \cos\theta_l \sin\theta_l = \sum_{l=1}^L \cos\theta_l = \sum_{l=1}^L \sin\theta_l = 0, \quad (9)$$

the elements of $\mathbf{M}$ can be found according to

$$\begin{aligned}
\boldsymbol{x}^{\mathsf{T}}\mathbf{R}^{-1}\boldsymbol{y} &= \sum_{i=1}^{N_s}\frac{\cos\theta_i\sin\theta_i}{\sigma_\eta^2 + 2kc^2\lambda^2} + \sum_{j=N_s+1}^{N}\frac{\cos\theta_j\sin\theta_j}{\sigma_\eta^2} = 0, \\
\boldsymbol{x}^{\mathsf{T}}\mathbf{R}^{-1}\mathbf{1}_N &= \sum_{i=1}^{N_s}\frac{\cos\theta_i}{\sigma_\eta^2 + 2kc^2\lambda^2} + \sum_{j=N_s+1}^{N}\frac{\cos\theta_j}{\sigma_\eta^2} = 0, \\
\boldsymbol{x}^{\mathsf{T}}\mathbf{R}^{-1}\boldsymbol{x} &= \sum_{i=1}^{N_s}\frac{\cos^2\theta_i}{\sigma_\eta^2 + 2kc^2\lambda^2} + \sum_{j=N_s+1}^{N}\frac{\cos^2\theta_j}{\sigma_\eta^2} \\
&= \frac{N_s}{2\left(\sigma_\eta^2 + 2kc^2\lambda^2\right)} + \frac{N - N_s}{2\sigma_\eta^2}, \\
\mathbf{1}_N^{\mathsf{T}}\mathbf{R}^{-1}\mathbf{1}_N &= \sum_{i=1}^{N_s}\frac{1}{\sigma_\eta^2 + 2kc^2\lambda^2} + \sum_{j=N_s+1}^{N}\frac{1}{\sigma_\eta^2} \\
&= \frac{N_s}{\sigma_\eta^2 + 2kc^2\lambda^2} + \frac{N - N_s}{\sigma_\eta^2}, \\
\boldsymbol{y}^{\mathsf{T}}\mathbf{R}^{-1}\boldsymbol{y} &= \boldsymbol{x}^{\mathsf{T}}\mathbf{R}^{-1}\boldsymbol{x}, \quad \boldsymbol{y}^{\mathsf{T}}\mathbf{R}^{-1}\mathbf{1}_N = \boldsymbol{x}^{\mathsf{T}}\mathbf{R}^{-1}\mathbf{1}_N.
\end{aligned}$$

Hence, the information matrix for the BTS configuration in (7) can be expressed as $\mathbf{M} = \frac{1}{\sigma_{\text{eq}}^2}\text{diag}\left[\frac{1}{2}\mathbf{I}_{2\times 2}, 1\right]$, where $\sigma_{\text{eq}}^2 \triangleq \frac{\left(\sigma_\eta^2+2kc^2\lambda^2\right)\sigma_\eta^2}{N\sigma_\eta^2+(N-N_s)2kc^2\lambda^2}$. Subsequently, given that (7) is the optimal configuration, the optimal estimation error covariance under sector clock bias discrepancies is

$$\mathbf{P}^\star \triangleq \text{diag}\left[\mathbf{P}_{x,y}^\star, \left(\sigma_{c\delta t_r}^\star\right)^2\right] = \sigma_{\text{eq}}^2\text{diag}\left[2\mathbf{I}_{2\times 2}, 1\right], \quad (10)$$

In order to demonstrate the result in (10), Monte Carlo (MC) simulations were conducted for several N_s and k values. The logarithm of the determinant of each resulting position estimation error covariance $\mathbf{P}_{x,y}$, namely $\log|\mathbf{P}_{x,y}|$ were plotted along with $\log\left|\mathbf{P}_{x,y}^\star\right|$ obtained in (10). A surface plot of $\log\left|\mathbf{P}_{x,y}^\star\right|$ and the MC simulation results for $\log|\mathbf{P}_{x,y}|$ are shown in Fig. 7.

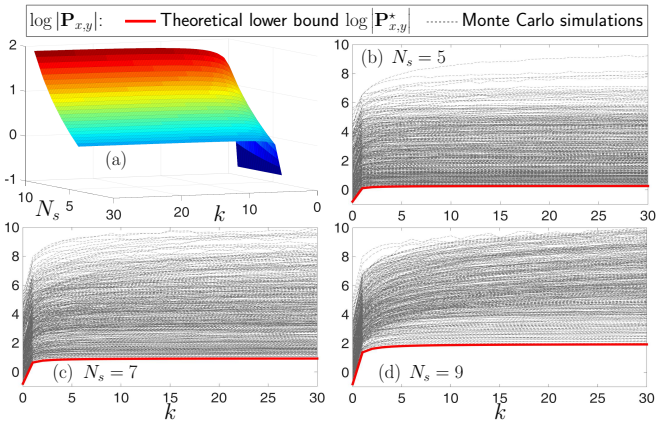

Fig. 7. (a) Surface plot of $\log\left|\mathbf{P}_{x,y}^\star\right|$ as a function of N_s and k. (b) Plots of $\log\left|\mathbf{P}_{x,y}\right|$ for 500 MC simulations along with the theoretical lower bound $\log\left|\mathbf{P}_{x,y}^\star\right|$. Simulation parameters: $N = 12$, $\sigma_\eta^2 = 4$ m^2, and $\lambda = 13$ ns.

The following can be concluded from these simulations. First, the expression in (10) is indeed the expression for the optimal estimation error covariance since $\log\left|\mathbf{P}_{x,y}^\star\right| \leq \log|\mathbf{P}_{x,y}|$ across all Monte Carlo runs. This validates the optimality of the configuration described in (7) with respect to minimizing the determinant of the estimation error covariance. Second, for a fixed $N_s < N$, $\log\left|\mathbf{P}_{x,y}^\star\right|$ becomes almost constant after five to ten time-steps and converges to a constant value that is calculated to be $\lim_{k\to\infty}\log\left|\mathbf{P}_{x,y}^\star\right| \approx \log\left[4\left(\frac{\sigma_\eta^2}{N-N_s}\right)^2\right]$. The same expression is obtained when the navigator uses only the measurements from the $N - N_s$ BTSs with no sector mismatch to estimate its state. This is attributed to the fact that the variance of the error in the measurements coming from the BTSs with sector mismatch is an affine function of time (cf. (6)). The uncertainty in these measurements will eventually become so large that these measurements will be "almost neglected" by the estimator. Moreover, the rate of increase of $\log\left|\mathbf{P}_{x,y}^\star\right|$ is proportional to $-\log\left[1-\frac{N_s}{N}+\frac{\sigma_\eta^2}{2kc^2\lambda^2}\right]$, and for relatively large k, this rate becomes proportional to $-\log\left[1-\frac{N_s}{N}\right]$, which approaches ∞ as N_s approaches N. It is therefore imperative to have at least one BTS with no sector mismatch in order for the estimation error covariance to be bounded.

V. Experimental Results

Navigation using the proposed mapper/navigator framework discussed in Section II was tested experimentally with the cellular CDMA SDR developed in [3]. For this purpose, a mapper was equipped with a high-gain tri-band cellular antenna and a surveyor-grade Leica GPS antenna. A DJI Matrice 600 unmanned aerial vehicle (UAV) was used as the navigator, which was equipped with a consumer-grade 800/1900 MHz cellular antenna and a small consumer-grade GPS antenna to discipline the on-board oscillator. The GPS and cellular signals on the mapper side were simultaneously down-mixed and synchronously sampled via a dual-channel universal software radio peripheral (USRP) driven by a GPS-disciplined oscillator (GPSDO). The cellular signals on the navigator side were down-mixed and sampled by a single-channel USRP also driven by a GPSDO. The cellular receivers were tuned to a 883.98 MHz carrier frequency, which is a channel allocated for the US cellular provider Verizon Wireless. Samples of the received signals were stored for off-line post-processing. The GPS signal was processed by a Generalized Radionavigation Interfusion Device (GRID) SDR [23] and the cellular CDMA signals were processed by the LabVIEW-based SDR proposed in [3]. The ground-truth reference for the navigator trajectory was taken from the UAV's on-board navigation system, which uses GPS, inertials, and other sensors. Fig. 8 shows the SOP BTS environment in which the mapper and navigator were present as well as the experimental hardware setup.

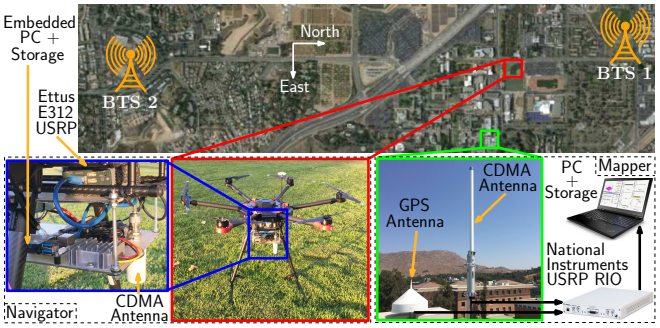

Fig. 8. SOP BTS environment and experimental hardware setup.

Over the course of the experiment, the mapper and the navigator were listening to the same 2 BTSs of which the position states were mapped prior to the experiment according to the framework discussed in [24]. The mapper was stationary during the experiments and was estimating the clock biases of the 2 known BTSs. In the absence of sector mismatch, the measurement noise variance for the mapper and navigator was calculated according to (2). Since only two BTSs were available for processing, an extended Kalman filter (EKF) framework was adopted (for observability considerations) to estimate the navigator's state. The navigator's position and velocity states were assumed to evolve according to velocity random walk dynamics and the clock bias and clock drift dynamics were modeled as a double integrator, driven by noise as discussed in [7]. The navigator was assumed

to be equipped with an oven-controlled crystal oscillator (OCXO) [17]. Two scenarios were tested in order to evaluate the proposed error model. In the first scenario, the mapper was forced to listen to a different sector of BTS1 than the navigator; however, the measurement noise covariance was not modified to compensate for the discrepancy introduced. The second scenario is similar to the first, except that the measurement noise covariance was modified to account for the sector clock bias discrepancy, as defined in (6). The navigator's true trajectory and estimated trajectory for each scenario are shown in Fig. 9. The position root-mean-square error (RMSE) for scenario 1 was found to be 23.99m, with a maximum position error of 38.93m and a standard deviation of 11.24m. For scenario 2, the position RMSE was found to be 13.48m with a maximum position error of 31.98m and a standard deviation of 5.19m. Fig. 9 shows a significant improvement in the estimation performance when the sector clock bias error model identified in this paper is used, which is reflected in a reduction of around 11m in the RMSE, 6m in the standard deviation, and 7m in the maximum error.

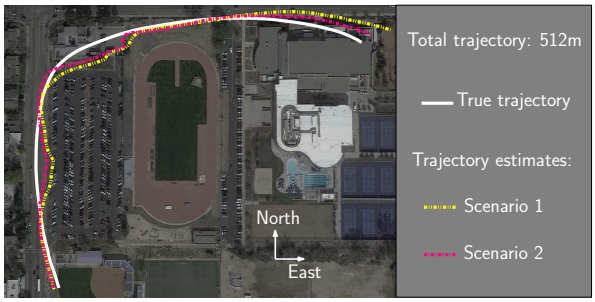

Fig. 9. Navigator's true and estimated trajectories.

VI. Conclusion

This paper studied the discrepancy between the clock biases of different sectors of the same BTS cell. This mismatch is harmful if it is unmodeled and accounted for appropriately in the navigation framework, should cellular signals be exploited for navigation, as it could result in errors on the order of tens of meters in the agent's position estimate and tens of nanoseconds in the agent's clock bias estimate. A stochastic dynamic model for this mismatch was identified and validated experimentally. The navigation performance under such error was analyzed by deriving the estimation error covariance with the minimum determinant, which was demonstrated against MC simulations. Moreover, experiments with a navigating UAV and a stationary mapper were conducted to test the navigation performance in two scenarios: (i) presence of discrepancies but without compensation and (ii) presence of discrepancies with compensation through the model derived in this paper. A reduction of approximately 11m in the UAV's position RMSE was achieved by compensating for the discrepancies with the model identified in the paper.

References

[1] S. Fang, J. Chen, H. Huang, and T. Lin, "Is FM a RF-based positioning solution in a metropolitan-scale environment? A probabilistic approach with radio measurements analysis," *IEEE Transactions on Broadcasting*, vol. 55, no. 3, pp. 577–588, September 2009.

[2] K. Pesyna, Z. Kassas, and T. Humphreys, "Constructing a continuous phase time history from TDMA signals for opportunistic navigation," in *Proceedings of IEEE/ION Position Location and Navigation Symposium*, April 2012, pp. 1209–1220.

[3] J. Khalife, K. Shamaei, and Z. Kassas, "A software-defined receiver architecture for cellular CDMA-based navigation," in *Proceedings of IEEE/ION Position, Location, and Navigation Symposium*, April 2016, pp. 816–826.

[4] J. Rufa and E. Atkins, "Sensor fusion for unmanned aircraft system navigation in an urban environment," in *Proceedings of American Control Conference*, June 2014, pp. 5313–5318.

[5] M. Rabinowitz and J. Spilker, Jr., "A new positioning system using television synchronization signals," *IEEE Transactions on Broadcasting*, vol. 51, no. 1, pp. 51–61, March 2005.

[6] R. Faragher, C. Sarno, and M. Newman, "Opportunistic radio SLAM for indoor navigation using smartphone sensors," in *Proceedings of IEEE/ION Position Location and Navigation Symposium*, April 2012, pp. 120–128.

[7] Z. Kassas and T. Humphreys, "Observability analysis of collaborative opportunistic navigation with pseudorange measurements," *IEEE Transactions on Intelligent Transportation Systems*, vol. 15, no. 1, pp. 260–273, February 2014.

[8] ——, "Motion planning for optimal information gathering in opportunistic navigation systems," in *Proceedings of AIAA Guidance, Navigation, and Control Conference*, August 2013, 551–4565.

[9] Z. Kassas, A. Arapostathis, and T. Humphreys, "Greedy motion planning for simultaneous signal landscape mapping and receiver localization," *IEEE Journal of Selected Topics in Signal Processing*, vol. 9, no. 2, pp. 247–258, March 2015.

[10] Z. Kassas and T. Humphreys, "Receding horizon trajectory optimization in opportunistic navigation environments," *IEEE Transactions on Aerospace and Electronic Systems*, vol. 51, no. 2, pp. 866–877, April 2015.

[11] ——, "The price of anarchy in active signal landscape map building," in *Proceedings of IEEE Global Conference on Signal and Information Processing*, December 2013, pp. 165–168.

[12] L. Merry, R. Faragher, and S. Schedin, "Comparison of opportunistic signals for localisation," in *Proceedings of IFAC Symposium on Intelligent Autonomous Vehicles*, September 2010, pp. 109–114.

[13] K. Pesyna, Z. Kassas, J. Bhatti, and T. Humphreys, "Tightly-coupled opportunistic navigation for deep urban and indoor positioning," in *Proceedings of ION GNSS Conference*, September 2011, pp. 3605–3617.

[14] C. Yang, T. Nguyen, and E. Blasch, "Mobile positioning via fusion of mixed signals of opportunity," *IEEE Aerospace and Electronic Systems Magazine*, vol. 29, no. 4, pp. 34–46, April 2014.

[15] J. Morales, P. Roysdon, and Z. Kassas, "Signals of opportunity aided inertial navigation," in *Proceedings of ION GNSS Conference*, September 2016, pp. 1492–1501.

[16] K. Shamaei, J. Khalife, and Z. Kassas, "Performance characterization of positioning in LTE systems," in *Proceedings of ION GNSS Conference*, September 2016, pp. 2262–2270.

[17] Z. Kassas, V. Ghadiok, and T. Humphreys, "Adaptive estimation of signals of opportunity," in *Proceedings of ION GNSS Conference*, September 2014, pp. 1679–1689.

[18] J. Khalife and Z. Kassas, "Characterization of sector clock biases in cellular CDMA systems," in *Proceedings of ION GNSS Conference*, September 2016, pp. 2281–2285.

[19] L. Ljung, *System identification: Theory for the user*, 2nd ed. Prentice Hall PTR, 1999.

[20] J. Proakis and D. Manolakis, *Digital signal processing*. Prentice-Hall, Upper Saddle River, NJ, 1996.

[21] R. Norton, "The double exponential distribution: Using calculus to find a maximum likelihood estimator," *The American Statistician*, vol. 38, no. 2, pp. 135–136, May 1984.

[22] N. Levanon, "Lowest GDOP in 2-D scenarios," *IEE Proceedings Radar, Sonar and Navigation*, vol. 147, no. 3, pp. 149–155, 2000.

[23] T. Humphreys, J. Bhatti, T. Pany, B. Ledvina, and B. O'Hanlon, "Exploiting multicore technology in software-defined GNSS receivers," in *Proceedings of ION GNSS Conference*, September 2009, pp. 326–338.

[24] J. Morales and Z. Kassas, "Optimal receiver placement for collaborative mapping of signals of opportunity," in *Proceedings of ION GNSS Conference*, September 2015, pp. 2362–2368.